Preprints (www.preprints.org) | NOT PEER-REVIEWED | Posted: 22 June 2022 doi:10.20944/preprints202110.0326.v2

Numerical Investigation of Cu_2O as a Hole Transport Layer for High-Efficiency, Cadmium Free CIGS solar cell

Muhammad Hassan Yousuf (M. H. Y)[1*], Faisal Saeed (F. S)[2,*], Haider Ali Tauqeer (H. A. T)[4]

[1]Department of Electrical Engineering, University of Engineering and Technology Lahore, Lahore, 5749, Punjab, Pakistan

[2]Department of Physics, Functional Materials and Optoelectronic Devics (FMOD) Lab, Lahore University of Management Sciences (LUMS), Lahore, 74792, Punjab Pakistan

[3]Department of Electrical Engineering, Lahore University of Management Sciences (LUMS), Lahore, 74792, Punjab Pakistan

M.H.Y-*2020msee137@student.uet.edu.pk, F.S-19060005@lums.edu.pk

ABSTRACT

The current research work is an effort to analyze the p-type Cu_2O layer as a hole transport layer on $Cu(In,Ga)Se_2$ (CIGS) absorber layer. The analysis is performed by utilizing the solar cell capacitance simulator, SCAPS-1D. Wideband and non-toxic ZnSe is employed as an n-type buffer layer along with Cu_2O. The simulation analyzes the thickness, defect density, and recombination in the absorber layer on photovoltaic properties of the solar cell. Moreover, the impact of various metal work functions is investigated as well. CIGS solar cell with Cu_2O as the hole transport layer and ZnSe buffer layer result in a high short circuit current density of 39.42 mA/cm^2 as compared to 34.73 mA/cm^2 measured in the reference cell without Cu_2O and the CdS buffer layer. Cu_2O enhances the conduction of photo-carriers (holes) at rare contact due to its p-type nature, hence, augmenting the device efficiency. The significant photocurrent enhancement in the UV region of the spectrum can be attributed to the lower parasitic absorption loss in ZnSe due to the larger bandgap of 2.9 eV, as compared to 2.4 eV of conventionally employed CdS. Overall, the solar cell conversion efficiency improved from 18.72% to 26.62% by adding a Cu_2O hole transport layer and substituting CdS with ZnSe. The results imply that Cu_2O is a promising hole transport material and the CIGS solar cell proposed in the current research effort may open new horizons for the development of high-efficiency thin-film solar cells.

Introduction

Thin-film copper indium gallium di-selenide [$Cu(In,Ga)Se_2$] or CIGS technology is considered the most promising next-generation photovoltaic (PV) technology due to its direct band-gap (~1.0-1.14 eV), high absorption coefficient (~ 10^5 cm^{-1}), and lower material losses [1-6].CIGS cells have the highest power conversion efficiency as compared to other thin-film technologies like Cu-chalcopyrite, cadmium telluride (CdTe), and amorphous silicon (a-Si), with a certified record efficiency of 23.40 % for lab-scale cells [7]. CIGS material is inexpensive and can deposit on any rigid or flexible substrate which increases its applications in commercial and wearable devices as well[8-10]. CIGS solar cells exhibit outstanding stability, high efficiencies and radiation tolerance hence can also be used for space application [11].

CIGS is a direct band-gap p-type semiconductor that minimizes the requirement of large diffusion length and also decreases losses. Such semiconductor with high absorption co-efficient is ideal for thin-film PV technology [12]. The tunable band-gap of p-type $CuIn_{1-x}Ga_xSe_2$ can be adjusted by varying the concentration of gallium and indium, to match the solar spectrum [13]. A thicker CIGS layer means more material which results in higher cost, particularly indium which is a costly material and its availability will be an issue in the future [14]. Aluminum (Al)/Nickle (Ni) and molybdenum (Mo) act as front and rear contact for the cell while Magnesium fluoride (MgF_2) acts as an anti-reflecting coating. Mo deposited on substrates offers lower electrical resistance (< 0.5 /sq.), higher thermal stability, and also less resistance to p-CIGS by forming a thin layer of molybdenum di-selenide ($MoSe_2$) during the absorber formation [15].

The optimum band gap for CIGS is ~ 1.14 eV due to material properties[16-17]. In general, for efficient absorption, a band-gap of ~ 1.4eV is required to match the solar spectrum. In CIGS crystal Indium can replaced by Gallium to achieve the required optical band gap, hence by the introduction of Indium the band-gap of CIGS can be varied from 1.04 eV to 1.7 eV.

Preprints (www.preprints.org) | NOT PEER-REVIEWED | Posted: 22 June 2022 doi:10.20944/preprints202110.0326.v2

Other elements can also be used in chalcopyrite $Cu(In,Ga,Al)(S,Se)_2$, this can vary band-gap from 1.04 eV ($CuInSe_2$) to about 3.5 eV ($CuAlS_2$) covering most of the visible spectrum. However, for CIGS material a higher band-gap causes complications. The efficiency of the cell decreases because of defect states and dangling bonds. For a wider band-gap, the defect level is in the middle of the band-gap thus increasing the band-gap also increases defect levels [18]. Fig. 1 [19] depicts a scanning electron microscope image (SEM) of a CIGS cell. In this substrate configuration, the light enters through a transparent conductive oxide (TCO) i.e., zinc oxide (ZnO) layer.

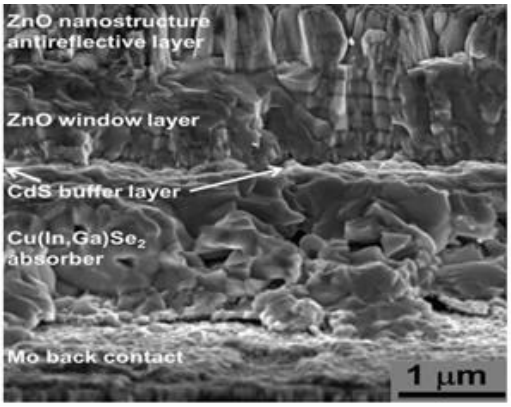

Figure 1. Scanning Electron Image (SEM) of buffer layered CIGS solar cell [19].

The working of CIGS cell is as follows: n-type cadmium sulfide (CdS) buffer layer (band-gap, $E_g \sim 2.4$ eV) absorbs the higher energy photons ≥2.4 eV, while photons of energy less than 2.4 eV are transmitted to the p-type CIGS absorber layer where electron-hole pairs are mainly generated. Due to the in-built junction voltage of n-CdS/p-CIGS, the electrons within the diffusion length are carried away from the p-CIGS layer to the n-CdS layer and are collected at the n-type electrode. Similarly, holes are carried away from the n-type buffer layer to the p-type absorber layer and are collected at the p-type electrode. A highly transparent, large band-gap (>3.3 eV) n-type TCO layer i.e., ZnO act as front contact over CdS called window layer. Typically, ZnO (E_g 3.2 eV) the layer consists of a double layer of a thick (400nm) layer of n-doped ZnO layer and a thin (50nm) intrinsic ZnO. The intrinsic-zinc oxide (i-ZnO) provides isolation between CdS and n-doped ZnO (ZnO: Al) so that i-ZnO prevents the diffusion of Al into the CdS/CIGS absorber layer.

The buffer layer acts as an intermediate layer between the window layer and absorber layer which provides stability [5, 20-21]. The buffer layer is highly-resistive and it prevents shunting between the absorber layer and TCO i.e., ZnO. The buffer layer affects the band offset and electric field in the junction, and thus improves the charge transport [22]. CdS is the most common material used as a buffer layer. The narrow band-gap of CdS causes current losses due to parasitic absorption. Additionally, cadmium (Cd) is a toxic element and is classified as a human carcinogen. For these reasons, extensive research is being done on the alternative buffer layer, such as Zinc sulfides, oxides, and selenides [23-26]. Like CdS, zinc selenide (ZnSe) is an n-type semiconductor but with a wide band-gap and the most promising material to replace CdS [27-30]. The band-gap of ZnSe is $E_g \sim$ 2.9 eV which is greater than the CdS $E_g \sim$2.4 eV, which means more light is passed to the CIGS absorber layer and a larger number of photo-carriers will be generated increasing efficiency.

This research effort proposes a theoretical approach to enhance the power conversion efficiency (PCE) of the CIGS solar cells with structure Substrate/Cu_2O/CIGS/buffer layer/intrinsic-i-ZnO/n-doped ZnO. The CIGS modeling and analyses are done by using a solar cell capacitance simulator (SCAPS-1D) that gives simulation results close to fabrication results [21, 31-35]. Here CdS is replaced with is replaced by a double buffer layer CdS/ZnSe. In addition to the double buffer layer, the Cu_2O is implemented as the hole transport layer (HTL). Cu_2O is an earth-abundant, non-toxic material and is easy to fabricate. The thickness of the CIGS absorber layer is reduced to 850 nm which is usually about 3000nm. Under standard illumination (AM1.5 G, 100 mW/cm^2, 300 K) [36], the photovoltaic parameters, short circuit current density (Jsc), open-circuit voltage (V_{oc}), fill factor (FF), and efficiency (η) of different hole transport layers and buffer layers under varied thicknesses are measured. Cu_2O is a p-type semiconductor and has an optical band-gap of 2.17 eV. Its application as photovoltaic material lies in the fact that the constituent materials are nontoxic and abundantly available on the earth, and that the Cu_2O has a high absorption coefficient in visible regions and low-cost. The doping concentration in Cu_2O can be achieved up to 10^{17} cm^{-3} [37].

Cuprite Cu_2O is known to have a low value of thermal expansion coefficient around room temperature, and to exhibits a negative thermal expansion behavior at low temperatures. The thermal decomposition temperature of Cu_2O exceeds 900 °C.

So, the high-temperature processing of CIGS material, may not have any serious effect on the Cu_2O layer [38]. Moreover, there is a possibility of Cu diffusion in CIGS material at the rear end which can change the CIGS band-gap and its performance. This can be addressed by the grading process of the CIGS structure and the exact band-gap of CIGS can be achieved from In/Ga ratio to compensate for Cu diffusion. As compared to conventional CIGS cells the device with Cu_2O as HTL gives greater output voltage. To optimize the light absorption and output current we put forward Cu_2O as HTL for further enhancement.

Theoretical studies show a significant increase in the efficiency of chalcopyrite-based solar cells with the introduction of Ga_2O_3, MoO_3, $MoSe_2$ and MoS_2 as back interfaces. MoO_3 gives maximum efficiency of 24 % among all due to its highest band-gap [39-41]. The band-gap of Cu_2O makes it suitable to work as a back interface for CIGS solar cells. Although for perovskite and copper zinc tin sulfide (CZTS) extensive studies are present on Cu_2O as HTL for CIGS, it's a novel approach. Here different parameters of CIGS cells are observed using SCAPS. It is observed by numerical calculations that Cu_2O increases the flow of charge carriers which greatly enhances the efficiency of CIGS cells. As compared to conventional CIGS cells the device with Cu_2O as HTL gives greater output voltage. By using Cu_2O recombination losses were reduced which results in high efficiency and stability. As Cu_2O is a transparent and inexpensive inorganic material it does not increase the cost and complexity of cell fabrication.

Materials and Methods

Numerical Modeling

Fig. 2 depicts the proposed CIGS solar cell with a p-type CIGS absorber layer and a thin layer of Mo deposited on a glass substrate. An n-type ZnSe material acts as a buffer layer and n-ZnO acts as a window layer. The proposed structure is simulated on SCAPS-1D software which solves semiconductor equations, the equation of continuity, and the Poisson equation for electrons and holes. These equations are as follows [42];

$$\frac{d^2}{dx^2}\psi(x) = \frac{e}{\varepsilon_0 \varepsilon_r}\left[\, p(x) - n(x) - N_a + N_d + p_t(x) - n_t(x) \,\right] \quad (1)$$

Where ψ is electrostatic potential, e is electric charge, ε_o, ε_r is the electric permittivity of vacuum and relative electric permittivity, p(x) and n(x) is the concentration of free holes and electrons, N_a, N_d are ionized acceptor and donor concentration, $p_t(x)$, $n_t(x)$ is the concentration of trapped holes and electrons.

$$\frac{\partial \Delta p}{\partial t} = G_P - \frac{\Delta p}{\tau_p} + D_p \frac{\partial^2 \Delta p}{\partial x^2} + \mu_P \frac{\partial E}{\partial x}\Delta p + \mu_P E \frac{\partial \Delta p}{\partial x} \quad (2)$$

$$\frac{\partial \Delta n}{\partial t} = G_n - \frac{\Delta n}{\tau_n} + D_n \frac{\partial^2 \Delta n}{\partial x^2} + \mu_n \frac{\partial E}{\partial x}\Delta n + \mu_n E \frac{\partial \Delta n}{\partial x} \quad (3)$$

Where $\partial\Delta p$, $\partial\Delta n$ is the change in holes and electron concentration, G is the generation rate of holes and electrons, τ_p ,τ_n is the hole and electron lifetime, D is the diffusion coefficient, μ_p ,μ_n is the mobility of holes and electrons and E is the electric field. SCAPS numerically calculates a steady-state solution of these equations with appropriate boundary conditions.

Material Parameters

The basic parameters used for the simulation of the proposed CIGS solar cell are shown in Table 1. The important parameter is the thickness of the absorber. It must be thick enough to absorb the highest cut-off wavelength of the incident solar radiation. For CIGS material thickness of 1-2 μm is enough to absorb the major portion of the visible spectrum. For this study, the CIGS layer is optimized to 850 nm for maximum efficiency. Apart from that, the thickness of the buffer layer is varied from 20 nm to 100 nm to observe the behavior and optimized to 50 nm for maximum efficiency. The Input parameters for device simulation were adopted from the experimental results, literature as well as self-ascribed [43-58].

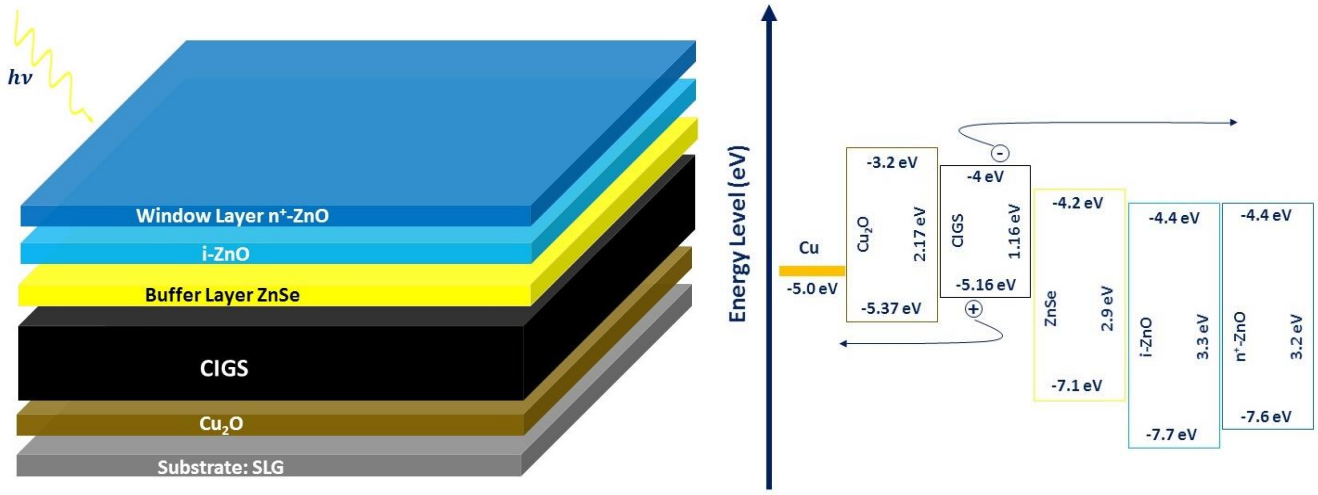

Figure 2. (a) Proposed CIGS solar cell architecture (b) Energy Band-gap diagram.

Table 1. Parameters for device simulation.

Parameters	Cu_2O	CIGS	ZnSe	i-ZnO	n^+-ZnO
Device Thickness (nm)	20	850	50 (Variable)	50	400
Band Gap (eV)	2.17	1.16	2.9	3.3	3.2
Electron Affinity (eV)	3.2	4.0	4.2	4.4	4.4
Dielectric Permittivity	7.1	13.6	10.0	9.0	9.0
CB Density of States (cm^{-3})	2×10^{17}	2×10^{17}	1×10^{18}	3.1×10^{18}	3.1×10^{18}
VB Density of States (cm^{-3})	1.1×10^{19}	1.5×10^{19}	1.8×10^{19}	1.8×10^{19}	1.8×10^{19}
Electron Mobility (cm^2/Vs)	200	100	70	100	100
Hole Mobility (cm^2/Vs)	80	25	3	31	31
Donor Density (cm^{-3})	0	0	5.5×10^{17}	1×10^{18}	1×10^{19}
Acceptor Density (cm^{-3})	1×10^{18}	1×10^{16}	0	0	0
Defect Density (cm^{-3})	1×10^{14}	1×10^{15}	1×10^{18}	1×10^{14}	1×10^{14}

Results and Discussion

Impact of Cu_2O Layer on device Performance

The J-V curve of both simulated cells was plotted, as shown in Fig 3. The electron-hole pair generated inside the absorber layer as light enters the cell are collected at respective electrodes. The J_{sc} of a solar cell is determined by the absorption coefficient, absorber layer thickness, and electron-hole mobility of the material. Apart from that suitable electron and hole selective layers play a critical role in the performance of the solar cell. As shown in Fig 3. the efficiency of CIGS cells greatly increases with the introduction of a thin layer of Cu_2O. The J_{sc} of 39.42 mA/cm^2, V_{oc} of 0.799 V, FF of 84.44 %, and PCE of 26.62 % are obtained for the cell with Cu_2O as compared to Jsc of 37.24 mA/cm2, Voc of 0.704 V for the device without Cu_2O. The hole mobility Cu_2O is 80 cm^2/Vs as compared to 25 cm^2/Vs for CIGS material. This results in the reduction of recombination of photo-generated carriers in the CIGS absorber layer thus increasing the number of carriers that contribute to photo-current which is also depicted in Fig 4. [46-47]. The wide band of Cu_2O reduces recombination losses and pulls holes from the CIGS absorber. This allows smoother extraction of holes with experiencing lower resistance. The proposed CIGS cell with HTL shows an increase in output, V_{oc}, and J_{sc}, as compared to cells without HTL and PCE increases from 18.72 to 26.62 %, a

total increase of 7.90 %, is recorded. This increase in efficiency can also be attributed to the p-type semiconductor nature of Cu_2O. The high absorption coefficient of Cu_2O allows for absorption of photons and contributes to photo current as recombination in this region is minimum. The absorption in Cu_2O can also be observed if the cell is simulated in an inverted manner.

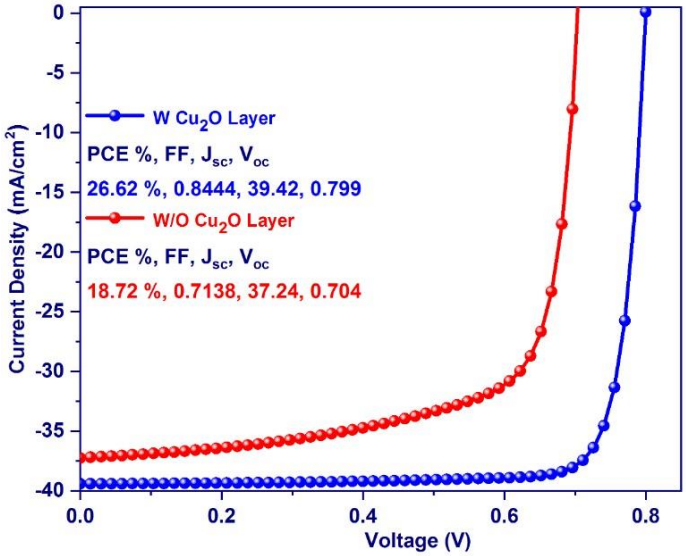

Figure 3. J-V curve of the simulated solar cells, with and without Cu_2O layer.

External Quantum Efficiency

External quantum efficiency (EQE) is the quantification of the spectral, optical, and electrical loss which determine the performance of a solar cell. Optical losses include transmission losses in the absorber layer (depending on band-gap), reflection at the surface and interfaces, and parasitic absorption losses in the functional layers. Additionally, a recombination of the minority carriers reduces the EQE. Recombination losses mainly dominate at the front surface and within the heavily doped emitter of solar cells [59-61]

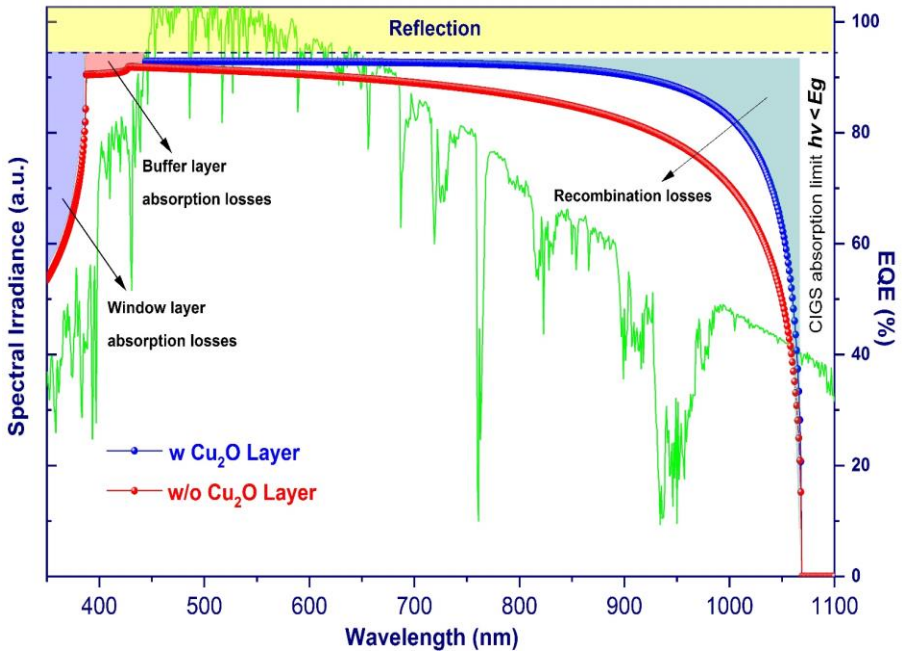

Figure 4. External Quantum Efficiency of the proposed CIGS solar cell.

Preprints (www.preprints.org) | NOT PEER-REVIEWED | Posted: 22 June 2022 doi:10.20944/preprints202110.0326.v2

Current solar cells have lower EQE at short wavelengths, λ<400 nm. In CIGS solar cells, parasitic absorption mainly occurs in the ZnO window and CdS buffer layers. Along with transmission and reflectance losses, the parasitic losses drastically reduce the short-wavelength EQE for λ<515 nm. This can be addressed by incorporating a luminescent down-shifting layer that is an efficient approach to enhancing the short-wavelength response of the solar cell. It absorbs short wavelength photons and re-emits longer wavelength photons, hence red-shifts the incident spectrum and improving the spectral response at short wavelength [62-63].

EQE of the simulated device at 350 nm wavelength (photon energy is 3.54 eV) is ~57.7 % and increased to ~90.79 % at the wavelength 450 nm (photon energy is 3.46 eV). The EQE remains above 80 % up to the wavelength of 1000 nm (photon energy of 1.23 eV). At short-wavelength 350 nm, such high EQE can attribute to the ZnSe buffer layer instead of the CdS layer that reduced EQE at a shorter wavelength. High EQE in the cell with a Cu_2O layer at a longer wavelength can attribute to the lower recombination inside the CIGS layer. As Cu_2O has higher hole mobility than CIGS material the holes move towards Cu_2O at a faster rate without recombination hence contributing to greater EQE.

Impact of CIGS Layer Thickness on device Performance

The CIGS layer thickness of the device depends on the concentration of the material, temperature, and vapor pressure during the fabrication. Therefore, it is essential to evaluate the device's performance at various absorber layer thicknesses. The CIGS layer thickness is variated from 0.1 m to 1.0 m, keeping all other device parameters intact. Corresponding results of the J–V curve, EQE, and PCE are summarized in Fig. 5. It is observed that on increasing the absorber layer thickness, the optical absorption of the material enhances which resulted in higher efficiency, especially at higher wavelengths, as depicted in Fig. 5(b). Since short-wavelength photons can absorb in a smaller thickness, the longer wavelength photons require a higher thickness absorber layer for complete absorption and reduce transmission losses.

Therefore, an increase in the thickness results in a higher absorption rate, lower transmittance loss, and greater charge carrier collection probability at higher wavelengths. Quantitatively, increasing the thickness from 100 nm to 1000 nm results in enhancement in EQE from 51.61% to 96.51% at wavelength 700 nm. Although an increase in the absorber layer thickness improves the optical performance of the device, absorption saturation restricts the improvement beyond a certain thickness which is also reflected in this study, where the beyond 400 nm thickness improvement in EQE is negligible, as depicted in Fig. 5(a). Enhanced optical performance anticipate the improvement in J_{sc}, an increase the thickness from 100 to 500 nm resulted in J_{sc} improvement from 20.23 mA/cm^2 to 37.46 mA/cm^2 whereas on increasing the thickness beyond 500 nm to 1000 nm resulted in 39.73 mA/cm^2. To this point, the impact on J_{sc} is analyzed whereas the device performance is the combination of all three parameters such as J_{sc}, V_{oc}, and FF. The PV parameters of the device show that the V_{oc} decreases up to 500 nm and then indicates saturation. This is attributed to the size of the absorber layer at a lower thickness the strength of the electric field is higher in the space charge region (SCR), hence resulting in higher V_{oc}. As the thickness increases, the ZnSe/CIGS and CIGS/Cu_2O interfaces move apart, and the associated electric field strength decreases which result in lower V_{oc}. Obtained FF improves up to 200 nm though decreases drastically at a thickness greater than 200 nm due to reduced electric field strength across the absorber layer. The PCE improves till 500 nm, beyond that only fractional improvement is observed which is attributed to the performance saturation of JV and EQE at a higher thickness of the CIGS absorber layer. This subsection concludes with a CIGS solar cell with a PCE of 26.62 % at the CIGS absorber layer thickness of 1000 nm. The same solar cell is studied under the influence of various defect levels in the CIGS in the following subsection.

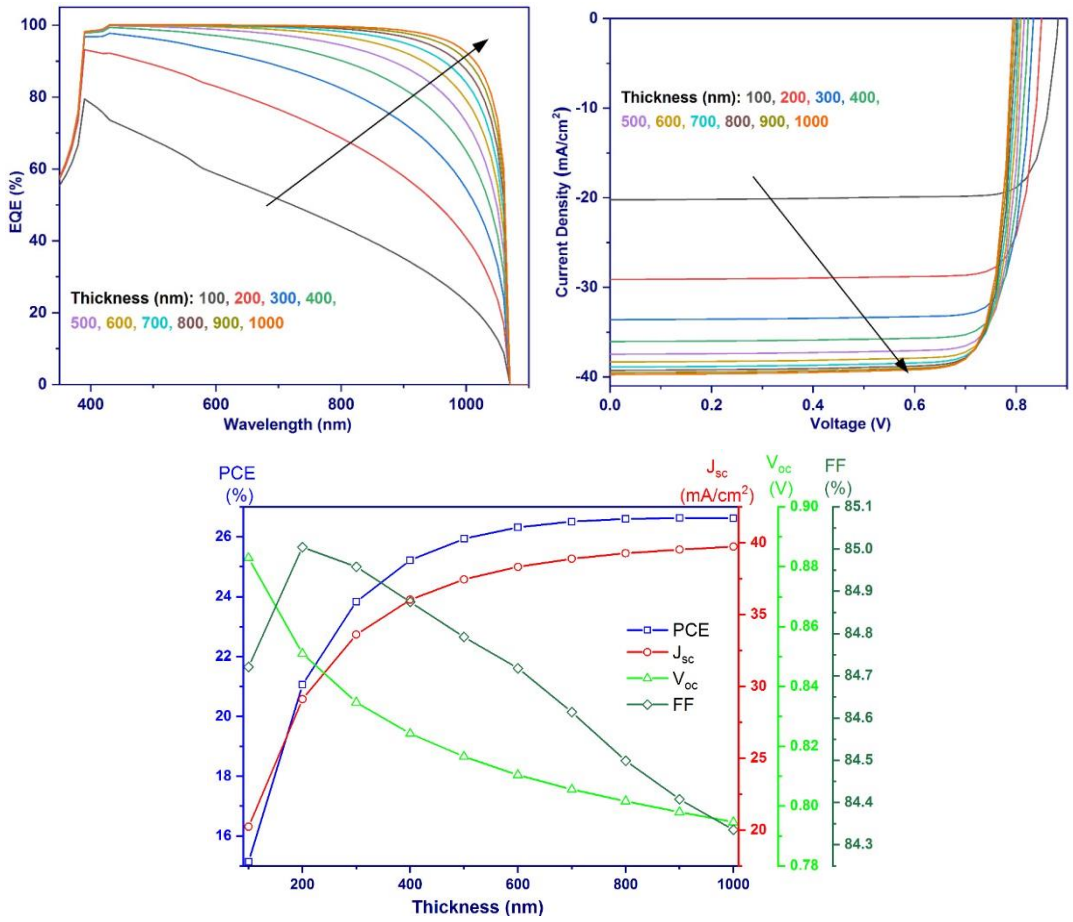

Figure 5. Impact of CIGS layer thickness on (a) EQE, (b) J–V curve, and (c) PV parameters of the device at various thicknesses, i.e., from 100 to 1000 nm. Results are obtained from the SCAPS-1D

Impact of defects in CIGS Layer on device Performance

The impact of defects in the CIGS absorber layer was also examined. In a semiconductor material defects are inevitable. In the CIGS material, defects exist as point defects i.e. lattice vacancy V_{Cu}, V_{In}, V_{Se}, intrinsic defects, and antisite defects like In_{Cu}, Cu_{In}, Ga_{Cu}, Cu_{Ga}. These defect are due to the p-type doping V_{Cu} and n-type doping V_{Se} or InCu [64-67]. These defects can also be an extended defect, such as a grain boundary-related defect, a dislocation, or a void and introduce deep or shallow levels in the energy band gap [68].

The Na diffusion from soda-lime glass (SLG) substrate to the CIGS layer increases the carrier concentration in the CIGS layer which leads to the formation of useful defect clusters that elevate CIGS material properties. Oana Cojocaru-Miredin et al. reported [69] that the atom probe tomography measurement shows a rich Na composition in the grain boundary that induced extended defects. L. E. Oikkonen et al. also reported [70] that two (Na-Na) Cu dumbbells attract each other, that means Na atoms can cluster together in a polycrystalline material. These cluster can appear at grain boundaries, causing an extended defects consisting of several (Na-Na) Cu dumbbells. The charge carriers can trap in these defects and facilitate nonradioactive electron-hole recombination.

Experimental results show the diffusion length of charge carriers is in the range of 0.5-2 μm in a CIGS material [71]. Since defect density is related to diffusion length [72]. Therefore, to see the effect of diffusion length on photovoltaic responses, the diffusion length of the electron was varied from 0.013 to 1.3 μm by varying the defect density from 10^{18} to 10^{14} cm^{-3} and results are illustrated in Fig. 6. The performance of the device improved as the defect density of the CIGS decreased. Heo, S. et al. [68] reported that via deep-level transient spectroscopy (DLTS) the defect in CIGS material is in the order of $\sim 10^{15}$. The

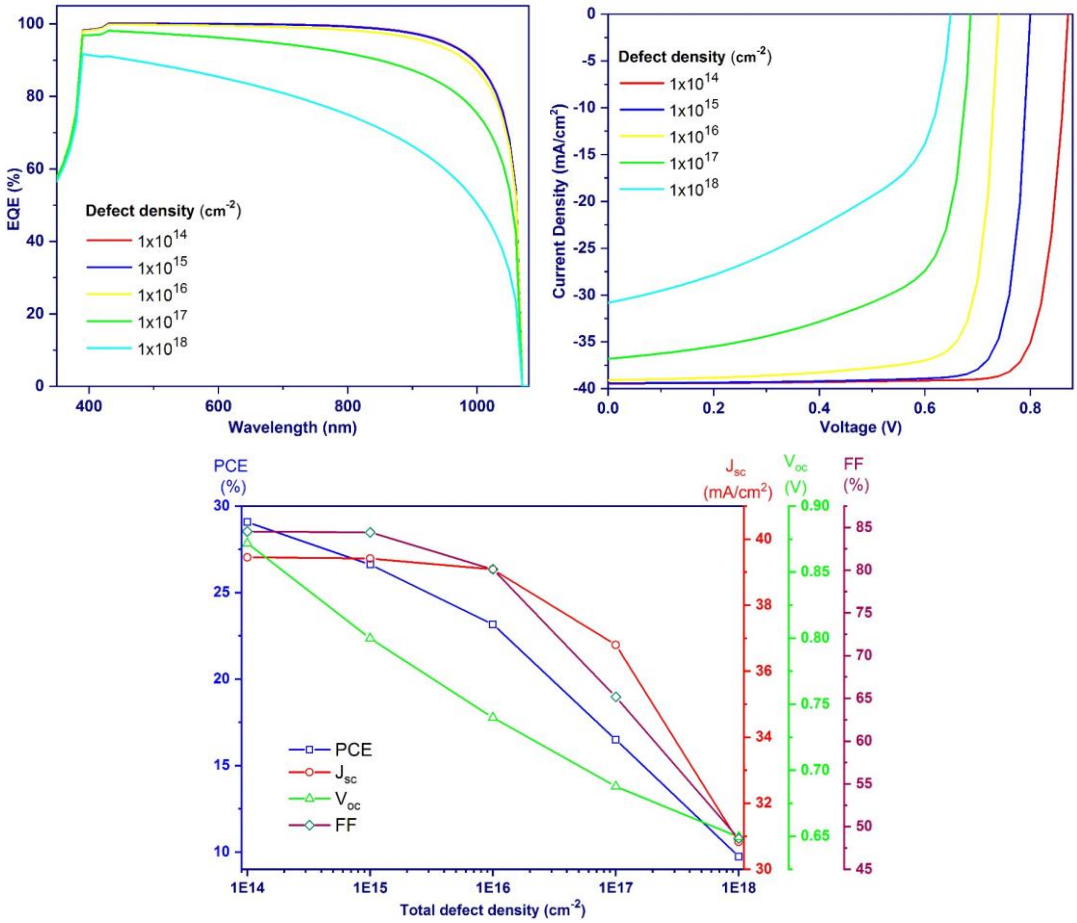

Figure 6. Impact of defect density in CIGS layer on (a) EQE, (b) J–V curve, and (c) PV parameters of the device at various Defect Density, i.e., from 10^{14} to 10^{18} nm. Results are obtained from the SCAPS-1D

initial defect density was set to be 1×10^{15} cm^3 as for such values of defect density the simulation results are realistic and close to experimental results. The simulated cell achieves the J_{sc} of 39.41 mA/cm^2, V_{oc} of 0.79 V, FF of 84.44% and PCE of 26.62 % at defect density of 10^{15} cm^3. As we further decrease N_t to 10^{14} cm^{-3}, variation in J_{sc} 39.45 mA/cm^2 and FF 84.53% is insignificant but for V_{oc} 0.87 V and PCE 29.07% a considerable change is observed. However, it is difficult to fabricate a semiconductor material with such a lower value of defect density in the lab.

Recombination Losses

The recombination losses in the CIGS solar cell are analyzed by employing Shockley–Read–Hall (SRH) recombination model. To analyze the recombination losses in the CIGS layer, the trap density N_t is varied from 10^{14} to 10^{18}. Figure 7 shows the impact of N_t on recombination rate at various values. It is observed that the recombination rate increases as defects in the device are increase consequently, PV parameters i.e. J_{sc}, V_{oc}, FF, and PCE of the solar cell decrease, as illustrated in Fig. 6. According to the SRH model, the recombination rate (R) can be expressed as;

$$R_{SRH} = \frac{1}{\tau_{n,p}} \times \frac{np - {n_i}^2}{p + n + 2n_i \cosh\left(\frac{E_i - E_t}{KT}\right)} \quad (4)$$

where, n, p, $\tau_{n,p}$, n_i, E_t and E_i are the density of electrons and holes, charge carrier lifetime (electron and hole), intrinsic density, energy level of defects and intrinsic energy level, respectively. The charge carrier lifetime is given by Equation 5

$$\tau = \frac{1}{\sigma_{n,p}\ v_{th}\ N_t} \tag{5}$$

where, $\sigma_{n,p}$, N_t and v_{th} are the charge carrier's capture cross-section, CIGS trap density, charge carrier velocity respectively. Following this equation, the recombination rate in the CIGS material increases by increasing the defects, as the lifetime of the charge carrier decrease as per Eq. 5. The diffusion length of charge carriers can be expressed as follows:

$$L_D = \sqrt{D\tau} \tag{6}$$

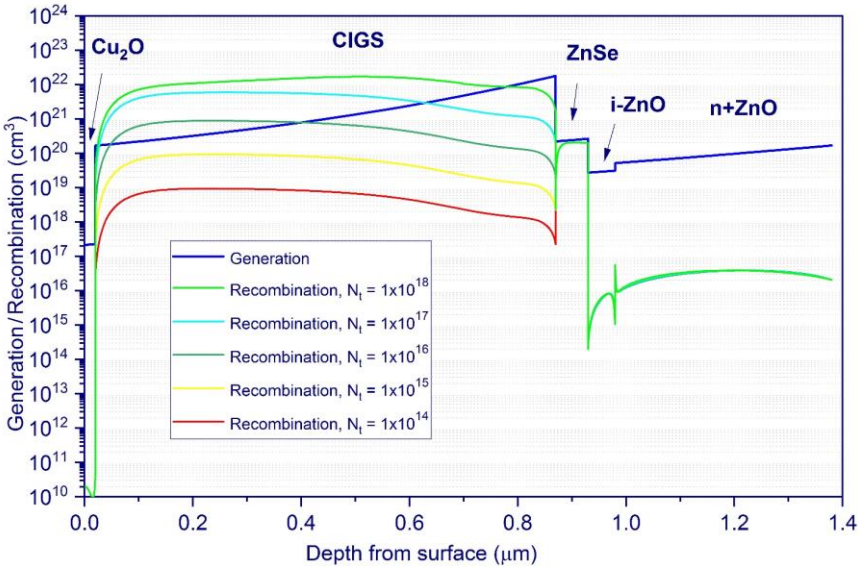

Figure 7. Generation, Recombination profile at various doping concentrations.

where, the diffusion coefficient D = (kt/q)μ. The diffusion coefficient is proportional to carrier mobility as for CIGS material the electron mobility is 100 cm^2/Vs and hole mobility is 25 cm^2/ Vs is large as experimentally observed [30,44]. Recombination in the Cu_2O is in the order of 10^{10} cm^3, least in the device whereas the generation rate is about 10^{17} cm^3. In the CIGS layer, the recombination rate increases from 10^{19} to 10^{22} as defect density varies from 10^{14} to 10^{18} which greatly affects the device performance whereas in the ZnO window layer recombination rate is 10^{17}, and the generation rate is 10^{20} hence it contributes to the device performance.

Optical Losses

For CIGS, the absorption coefficient, α in the photon energy range $h<E_g$ is $\alpha=4\pi k/\lambda$= (4-5) $\times 10^3$ cm^{-1} [48]. These values of α should result in a high value of quantum efficiency but this is not observed in this case. For $\lambda>\lambda_g=hc/E_g$ the quantum efficiency decreases drastically to zero within a range of 100 nm above λ_g. This rapid decrease in quantum efficiency can be attributed to the 'band tails' of the density of states which is due to disordered crystal structures and strong doping in the semiconductor. The force field of the impurity atom and wave function of electrons overlap and transformed into an impurity band. At critical concentration, the conduction band joins with the impurity band which results in tails of the density of states.
The absorption coefficient depends exponentially on incident photon energy shown as follows;

$$\alpha = \alpha_0 \exp\left[\frac{h\nu - E_0}{E_U\ T}\right] \tag{7}$$

Where E_U is Urbach energy, these empirical dependencies are represented by the Urbach rule [49]. For an electron to take part in photo generated current it must absorb energy greater than or equal to E_g. In the case of tail absorption at $h<E_g$, the electron gets energy equal to h from the incident photon and the rest is covered by phonons. The Urbach rule represents that as hv decreases, the probability of the multi-phonon process also decreases. The electron absorbed a photon having energy hv

< E_g takes part in photocurrent just as that of h≥E_g. The part of spectrum hv < E_g makes a small contribution to short circuit current 0.40 mA/cm^2 (1.10%). For spectral range h≥E_g absorption coefficient follows the direct-band-gap law for semiconductors expressed as follows;

$$\alpha = \alpha_0 \frac{\sqrt{hv - E_g}}{hv} \tag{8}$$

For CIGS material with a bandgap E_g=1.16 eV, the wavelength is given by, λ_g= hc/E_g=1068 nm. Optical losses can be calculated quantitively by calculating short circuit current density J_{sc}. If hv is the photon energy and φ_i is the spectral radiation power density, J_{sc} can be written as follows. 9

$$J_{sc} = q \sum_i \frac{\phi_i \lambda_i}{hv} T(\lambda_i)\, \eta\, \Delta\lambda_i \tag{9}$$

Where q is the charge on the electron, is the quantum efficiency here assumes =1, T(λ_i) is the transmission of photons from one layer to the other, the summation in the above equation should range from =300 nm to λ_g= hc/E_g= 1068 nm for bandgap E_g=1.16 eV. For such CIGS cells, the total reflection losses are about 8.1% and total absorption losses are 9.4% which adds up to 17.5% of total optical losses.

Metal contact work function

To examine the contact nature of metal contact/HTL interface, a work function study was conducted on various metals. The studied metals are Mo, Ag, Fe, Cu, Au, and Pt, having metal work function 4.6 eV, 4.74 eV, 4.81 eV, 5.0 eV, 5.10 eV, and 5.70 eV, respectively. Figure 8 a, b. shows an energy band diagram for various metals which shows that the barrier height increases as the work function of contact materials decrease. Figure 9 a, b. shows an impact of metal work function on the PV parameters. It is evident that the PCE decreases as the metal work function decreases. For the Mo, Ag, Fe, Cu, and Au, a Schottky contact was established as the work function is less than the work function of Cu_2O. However, for Pt, an ohmic contact was established at the metal/Cu_2O interface as the work function is greater than Cu_2O. Figure 9 a, b. shows the effect of work function on the FF and PCE of the device. It is observed that PV parameters increase from 4.6 eV to 4.9 eV and then saturate. This can be attributed to the work function of Cu_2O being about ~5.0 eV which is close to Cu [73]. Hence at 5.0 eV and above the efficiency of the device is maximum. Cu_2O layer is deposited by the high-temperature oxidation of a thin sheet of Cu and therefore it is an efficient option for rare contact.

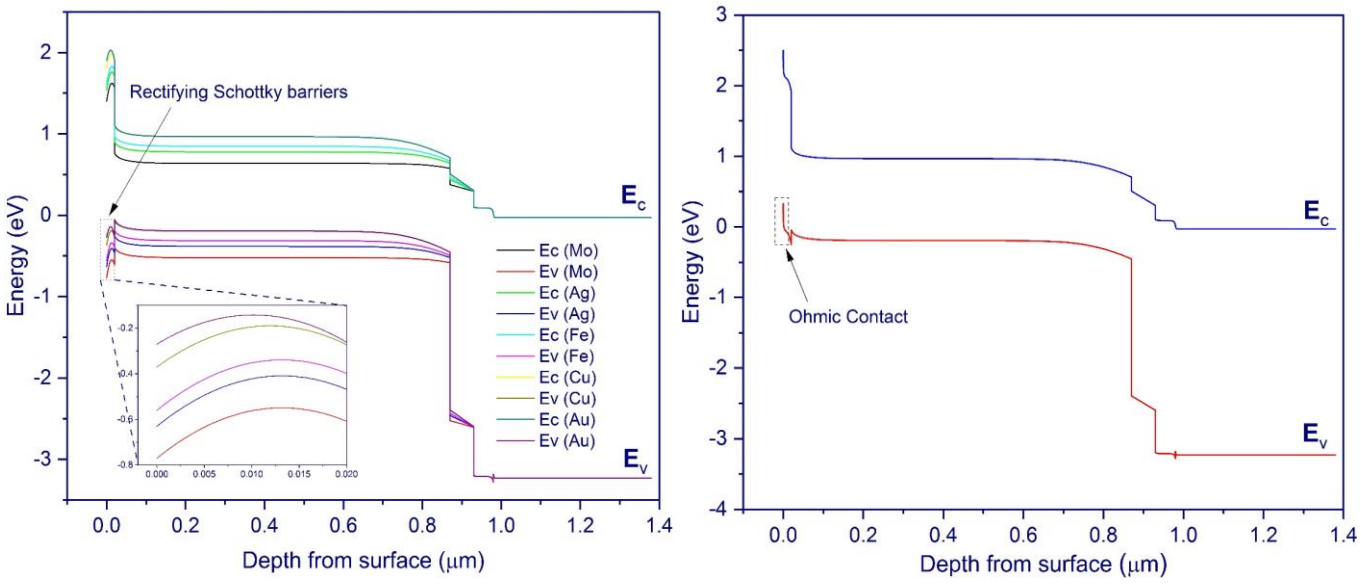

Figure 8. (a) Schottky contact, (b) Ohmic contact

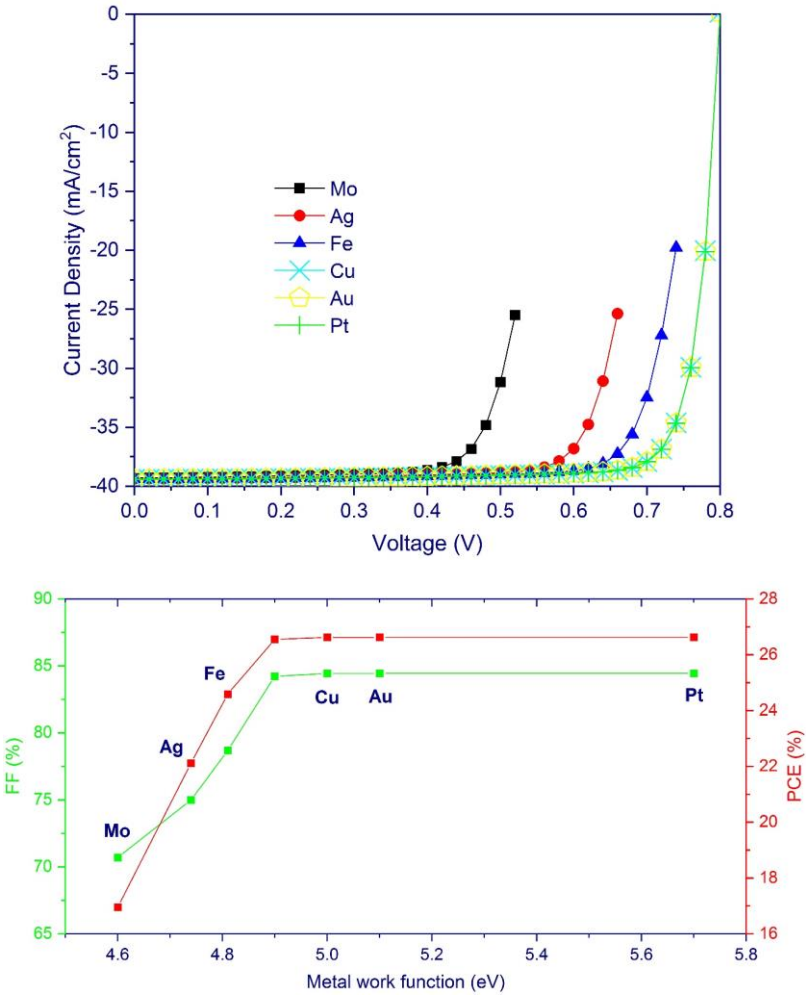

Figure 9. (a) J-V curve for various metals and (b) FF, PCE vs Metal work function

Results Comparison

Table 2. shows a comparison of basic photovoltaic parameters among conventional buffer layers of CdS, ZnSe, CdS/ZnSe double buffer layer, and ZnSe along with Cu_2O as a hole transport layer. The PCE of CIGS cells with Cu_2O is much larger than conventional CIGS cells. As compared to the solar cells with only CdS as buffer layer 18.72% and with CdS/ZnSe as double buffer layer 19.01 %. with the introduction of Cu_2O as HTL, the overall efficiency increases up to 26.63 %.

Table 2. Summary of the photovoltaic parameters of all the devices considered in this study.

Device	J_{sc} (mA/cm^2)	V_{oc} (V)	FF (%)	PCE (%)	Ref
Proposed CIGS Solar Cell (with Cu_2O and ZnSe)	39.42	0.799	84.44	26.62	This work
CIGS Solar cell without Cu_2O	37.24	0.704	71.38	18.72	This work
CIGS Solar cell with CdS buffer layer	34.77	0.68	77.49	18.72	Moradi. et al. [54]
CIGS Solar cell with ZnSe Buffer layer	33.42	0.746	71.78	17.92	Wang, H. et al. [53]
CIGS Solar cell with CdS/ZnSe Buffer layer	33.94	0.744	75.2	19.01	Wang, H. et al. [53]

Conclusion

The paper concludes with a 26.62% efficient CIGS solar cell design through comprehensive device simulations. A compendious analysis of the CIGS cell is executed in terms of variation in the CIGS absorber layer thickness and defect density (per experimental data) to optimize the device performance. Furthermore, Cu_2O as the hole transport layer and ZnSe as buffer layers are examined as well. The thickness of these layers was optimized to achieve maximum efficiency. The performance of the device is greatly enhanced with the Cu_2O layer at the rare contact. This can be attributed to mainly two factors i) the transmission of photo-carriers reduces the carrier recombination at rare contact which allows smoother extraction of holes while experiencing lower resistance, and ii) the wide bandgap of the ZnSe buffer layer authorize a larger number of photons to pass and absorb in the CIGS layer. Therefore, the current CIGS design delivers a J_{SC} of 39.42 mA/cm^{-2} and a V_{OC} of 0.799 V, leading to an optimum design. Metalwork function analysis depicts that Cu along with Cu_2O HTL delivers pinnacle results instead of Mo rear contact. As Cu_2O can be produced by the oxidation of Cu which presents high thermal stability; making it an optimal choice alongside CIGS material. The results present the effectiveness of HTL by confirming the enhancement of efficiency as a result of the curtailment of the recombination losses in the absorber layer. CIGS solar cells have lower lab-scale efficiency of about 25% than Si-cells. The current effort presents an increase in the efficiency with the addition of Cu_2O. Based on the results, it is expected that CIGS cells with HTL can be a breakthrough in the solar industry due to higher efficiency as well as stability.

Funding: This work was supported by Taif University Researchers Supporting Project number (TURSP-2020/144), Taif University, Taif, Saudi Arabia.

References

[1] F. Ahmad, T. H. Anderson, P. B. Monk, and A. J. A. o. Lakhtakia, "Efficiency enhancement of ultrathin CIGS solar cells by optimal band gap grading, *Applied Optics*, 58(22), 6067-6078 (2019).

[2] Y.-J. J. O. e. Chang, "Suppressing lossy-film-induced angular mismatches between reflectance and transmittance extrema: optimum optical designs of inter layers and AR coating for maximum transmittance into active layers of CIGS solar cells: *erratum*,*Opt Express*, 23, A947-A948 (2015).

[3] I. Massiot, A. Cattoni, and S. J. N. E. Collin, "Progress and prospects for ultrathin solar cells, *Nature Energy*, 5, 959-972 (2020).

[4] C. Onwudinanti, R. Vismara, O. Isabella, L. Grenet, F. Emieux, and M. J. O. e. Zeman, "Advanced light management based on periodic textures for Cu (In, Ga) Se 2 thin-film solar cells,*Optics Express* 24, A693-A707 (2016).

[5] S. Shi, L. Yao, P. Ma, Y. Jiao, X. Zheng, D. Ning, M. Chen, F. Sui, H. Liu, and C. J. M. T. E. Yang, "Recent progress in high temperature resistance PI substrate with low CTE for CIGS thin film solar cells,*Materialtoday Energy*,20, 100640 (2021).

[6] R. Tang, X. Wang, W. Lian, J. Huang, Q. Wei, M. Huang, Y. Yin, C. Jiang, S. Yang, and G. J. N. E. Xing, "Hydrothermal deposition of antimony selenosulfide thin films enables solar cells with 10% efficiency,*Nature energy*, 5, 587-595 (2020).

[7] D. Aiken, E. Dons, S.-S. Je, N. Miller, F. Newman, P. Patel, and J. J. I. J. o. P. Spann, "Lattice-Matched Solar Cells with 40% Average Efficiency in Pilot Production and a Roadmap to 50%," *IEEE Journal of Photovoltaics*, 3, 542-547, Jan. 2013

[8] S. Cao, D. Yu, Y. Lin, C. Zhang, L. Lu, M. Yin, X. Zhu, X. Chen, D. J. A. a. m. Li, , "Light Propagation in Flexible Thin-Film Amorphous Silicon Solar Cells with Nanotextured Metal Back Reflectors,*ACS Appl. Mater. Interfaces*, 12, 26184-26192 (2020).

[9] A. Chirila, P. Reinhard, F. Pianezzi, P. Bloesch, A. R. Uhl, C. Fella, L. Kranz, D. Keller, C. Gretener, and H. J. N. m.˘ Hagendorfer, "Potassium-induced surface modification of Cu (In, Ga) Se 2 thin films for high-efficiency solar cells,*Nature materials*, 12, 1107-1111 (2013).

[10] K.-J. Yang, S. Kim, S.-Y. Kim, K. Ahn, D.-H. Son, S.-H. Kim, S.-J. Lee, Y.-I. Kim, S.-N. Park, and S.-J. J. N. c. Sung, "Flexible Cu 2 ZnSn (S, Se) 4 solar cells with over 10% efficiency and methods of enlarging the cell area,*Nature communications* 10, 1-10 (2019).

[11] P. Reinhard et al., "Cu(In,Ga)Se_2 Thin-Film Solar Cells and Modules—A Boost in Efficiency Due to Potassium," *IEEE Journal of Photovoltaics*, 5, 2, 656-663, March 2015

[12] A. Bouloufa, K. Djessas, and A. J. T. S. F. Zegadi, "Numerical simulation of CuIn sub x Ga sub 1-x Se sub 2 solar cells by AMPS-1D, *Thin Solid Films*, 515,15, 6285-6287 (2007).

[13] M. Latha, R. A. Devi, and S. J. O. M. Velumani, "Hot injection synthesis of Cu (In, Ga) Se2 nanocrystals with tunable bandgap,*Optical Materials*, 79, 450-456 (2018).

[14] K. Ramanathan, R. Noufi, B. To, D. Young, R. Bhattacharya, M. Contreras, R. Dhere, and G. Teeter, "Processing and properties of sub-micron CIGS solar cells, *IEEE 4th World Conference on Photovoltaic Energy*, (IEEE, 2006), 380-383.

[15] S. R. Kodigala, "Cu (In1 xGax) Se2 and CuIn (Se1 xSx) 2 Thin Film Solar Cells," *Thin films and nanostructures*, 35, 505-679.

[16] S. Gharibzadeh, I. M. Hossain, P. Fassl, B. A. Nejand, T. Abzieher, M. Schultes, E. Ahlswede, P. Jackson, M. Powalla, and S. J. A. F. M. Schäfer, "2D/3D Heterostructure for Semitransparent Perovskite Solar Cells with Engineered Bandgap Enables
Efficiencies Exceeding 25% in Four-Terminal Tandems with Silicon and CIGS, *Advanced funcntional material*, 30, 1909919 (2020).

[17] Y. Kamikawa, J. Nishinaga, H. Shibata, S. J. A. A. M. Ishizuka, and Interfaces, "Efficient Narrow Band Gap Cu (In, Ga) Se2 Solar Cells with Flat Surface, *ACS Appl. Mater. Interfaces*, 12, 45485-45492 (2020).

[18] J. Ramanujam, U. P. J. E. Singh, and E. Science, "Copper indium gallium selenide based solar cells–a review,*Energy environmental science*, 10, 1306-1319 (2017).

[19] Y. J. N. S. C. Tang, "Copper indium gallium selenide thin film solar cells,*Nanostructured Solar Cells*, 183-200 (2017).

[20] Q. Du, B. Li, S. Shi, K. Zhang, Y. Zhang, S. Cheng, Z. Zhou, F. Liu, S. Sun, and Y. J. C. Sun, "Relationship between the intermediate phases of the sputtered Zn (O, S) buffer layer and the conduction band offset in Cd-free Cu (In, Ga) Se 2 solar cells,*CrystEngcomm*, 22, 4416-4426 (2020).

[21] L. Wang, D.-B. Li, K. Li, C. Chen, H.-X. Deng, L. Gao, Y. Zhao, F. Jiang, L. Li, and F. J. N. E. Huang, "Stable 6%-efficient Sb 2 Se 3 solar cells with a ZnO buffer layer,*Nature energy*, 2, 1-9 (2017).

[22] A. O. Pudov, "Impact of secondary barriers on copper-indium-gallium-selenide solar-cell operation,*Colorado State University Publication Number: AAI3173082; ISBN: 9780542099502*; (Colorado State University, 2005).

[23] T. Feurer, P. Reinhard, E. Avancini, B. Bissig, J. Löckinger, P. Fuchs, R. Carron, T. P. Weiss, J. Perrenoud, S. J. P. i. P. R. Stutterheim, and Applications, "Progress in thin film CIGS photovoltaics–Research and development, manufacturing, and applications,*Progress in Photovoltaic*, 25, 645-667 (2017).

[24] C. Huang, S. S. Li, W. Shafarman, C.-H. Chang, E. Lambers, L. Rieth, J. Johnson, S. Kim, B. Stanbery, T. J. S. e. m. Anderson, and s. cells, "Study of Cd-free buffer layers using Inx (OH, S) y on CIGS solar cells,*Solar Energy Materials and Solar Cells*, 69, 131-137 (2001).

[25] X. Y. Kong, D. Yu, Z. Huang, W. Shen, and N. Dai, "Atomic layer deposition for photovoltaic: applications and prospects, *Optical Nanostructures and Advanced Materials for Photovoltaics*, (Optical Society of America, 2015)

[26] N. Mufti, T. Amrillah, A. Taufiq, M. Diantoro, and H. J. S. E. Nur, "Review of CIGS-based solar cells manufacturing by structural engineering*Solar Energy*,207, 1146-1157 (2020).

[27] A. Ashok, G. Regmi, A. Romero-Núñez, M. Solis-López, S. Velumani, and H. J. J. o. M. S. M. i. E. Castaneda, "Comparative studies of CdS thin films by chemical bath deposition techniques as a buffer layer for solar cell applications,*Journal of Materials Science: Materials in Electronics* , 31 1-20 (2020).

[28] F. Ghamsari-Yazdel, I. Gharibshahian, and S. J. J. o. M. S. M. i. E. Sharbati, "Thin oxide buffer layers for avoiding leaks in CIGS solar cells; a theoretical analysis,*Journal of Materials Science: Materials in Electronics*,32, 1-11 (2021).

[29] R. Sharma, S. Patel, S. Chander, M. Kannan, and M. J. P. L. A. Dhaka, "Physical properties of ZnSe thin films: Air and vacuum annealing evolution to buffer layer applications,*Physics Letters A*, 384, 126097 (2020).

[30] F. Takagi, Y. Kageshima, K. Teshima, K. Domen, H. J. S. E. Nishikiori, and Fuels, "Enhanced photoelectrochemical performance from particulate ZnSe: Cu (In, Ga) Se 2 photocathodes during solar hydrogen production via particle size control,*Sustainable energy fuels*, 5, 412-423 (2021).

[31] I. M. De Los Santos, H. J. Cortina-Marrero, M. Ruíz-Sánchez, L. Hechavarría-Difur, F. Sánchez-Rodríguez, M. Courel, and H. J. S. E. Hu, "Optimization of CH3NH3PbI3 perovskite solar cells: A theoretical and experimental study,*Solar Energy*, 199, 198-205 (2020).

[32] L. Et-taya, T. Ouslimane, and A. J. S. E. Benami, "Numerical analysis of earth-abundant Cu2ZnSn (SxSe1-x) 4 solar cells based on Spectroscopic Ellipsometry results by using SCAPS-1D, *Solar Energy*,201, 827-835 (2020).

[33] B. K. Mondal, S. K. Mostaque, M. A. Rashid, A. Kuddus, H. Shirai, J. J. S. Hossain, and Microstructures, "Effect of CdS and In3Se4 BSF Layers on the photovoltaic performance of PEDOT: PSS/n-Si Solar Cells: Simulation based on experimental data,*Superlattices and Microstructures*, 106853 (2021).

[34] M. K. S. B. Rafiq, N. Amin, H. F. Alharbi, M. Luqman, A. Ayob, Y. S. Alharthi, N. H. Alharthi, B. Bais, and M. J. S. r. Akhtaruzzaman, "WS 2: a new window layer material for solar cell application,*Scientific Reports*, 10, 1-11 (2020).

[35] A. F. F. Violas, "Novel Rear Contact Architectures in CIGS Solar Cells: Modelling and Experimental Fabrication,*FCT: DCM - Dissertações de Mestrado*, (2020).

[36] X. Liu, Y. Wang, T. Wu, X. He, X. Meng, J. Barbaud, H. Chen, H. Segawa, X. Yang, and L. J. N. c. Han, "Efficient and stable tin perovskite solar cells enabled by amorphous-polycrystalline structure,*Nature communications*, 11, 1-7 (2020).

[37] K. Akimoto, S. Ishizuka, M. Yanagita, Y. Nawa, Goutam K. Paul, T. Sakurai, Thin film deposition of Cu2O and application for solar cells,*Solar Energy*, 80, 6, 2006, Pages 715-722

[38] Zeshunji Luo, Licai Fu, Jiajun Zhu, Wulin Yang, Deyi Li, Lingping Zhou, Cu2O as a promising cathode with high specific capacity for thermal battery, *Journal of Power Sources*, 448, 2020,227569, ISSN 0378-7753,

[39] Tokio Nakada, Microstructural and diffusion properties of CIGS thin film solar cells fabricated using transparent conducting oxide back contacts, *Thin Solid Films*, 480–481, 2005, Pages 419-425, ISSN 0040-6090,

[40] Jürgen H. Werner, Julian Mattheis, Uwe Rau, Efficiency limitations of polycrystalline thin film solar cells: case of Cu(In,Ga)Se2, *Thin Solid Films*, 480–481, 2005, 399-409, ISSN 0040-6090,

[41] Weimin Li, Wenjie Li, Ye Feng, Chunlei Yang, Numerical analysis of the back interface for high efficiency wide band gap chalcopyrite solar cells, Solar Energy, 180, 2019, 207-215, ISSN 0038-092X,

[42] A. Lachgueur and K. Rahmoun, "Simulation and Analysis of Perovskite Solar Cell Based on Germanium," *ICREEC* (Springer, 2020), 407-412.

[43] L. Lin, L. Jiang, P. Li, B. Fan, Y. J. J. o. P. Qiu, and C. o. Solids, "A modeled perovskite solar cell structure with a Cu2O hole-transporting layer enabling over 20 % efficiency by low-cost low-temperature processing,*Journal of Physics and Chemistry of Solids*, 124, 205-211 (2019).

[44] Patel, P.K. Device simulation of highly efficient eco-friendly CH3NH3SnI3 perovskite solar cell. Sci Rep 11, 3082 (2021). https://doi.org/10.1038/s41598-021-82817-w

[45] Qu, J., Zhang, L., Wang, H. et al. Simulation of double buffer layer on CIGS solar cell with SCAPS software. Opt Quant Electron, *Optical and Quantum Electronics*, 51, 383 (2019). https://doi.org/10.1007/s11082-019-2100-9

[46] J. P. Teixeira, R. B. Vieira, B. P. Falcao, M. Edoff, P. M. Salome, and J. P. J. T. J. o. P. C. C. Leitao, "Recombination Channels in Cu (In, Ga) Se2 Thin Films: Impact of the Ga-Profile,*J. Phys. Chem. C*, 124, 12295-12304 (2020).

[47] L. Zhang, T. Li, Y. Chen, W. Pang, M. Qu, X. Song, Y. Zhang, and H. J. J. o. M. S. M. i. E. Yan, "Influences of donor defect passivation on the performance of Cu (In, Ga) Se 2 thin-film solar cell,*Journal of Materials Science: Materials in Electronics*, 29, 3482-3491 (2018)

[48] P. D. Paulson, R. Birkmire, and W. J. J. o. A. P. Shafarman, "Optical characterization of CuIn 1 x Ga x Se 2 alloy thin films by spectroscopic ellipsometry, *Journal of Applied Physics*, 94, 879-888 (2003).

[49] J. D. Dow, "Urbach's Rule, *Optical Properties of Highly Transparent Solids*, (Springer, 1975), 131-143.

[50] K. Puech, S. Zott, K. Leo, M. Ruckh, and H. W. J. A. p. l. Schock, "Determination of minority carrier lifetimes in CuInSe2 thin films,*Appl. Phys. Lett*, 69, 3375- 77 (1996).

[51] C. S. Solanki, Solar photovoltaics: fundamentals, technologies and applications (Phi learning pvt. Ltd., 2015).

[52] K. J. Z. f. P. Hecht, "Zum Mechanismus des lichtelektrischen Primärstromes in isolierenden Kristallen,*Zeitschrift für Physik*, 77, 235-245 (1932).

[53] Qu, J., Zhang, L., Wang, H. et al. Simulation of double buffer layer on CIGS solar cell with SCAPS software. Opt Quant Electron, *Optical and Quantum Electronics*, 51, 383 (2019). https://doi.org/10.1007/s11082-019-2100-9

[54] DTakahito Nishimura a, Jakapan Chantana b,c, Abdurashid Mavlonov b, Yu Kawano c, Taizo Masuda d,e, Takashi Minemoto Minemoto, evice design for high-performance bifacial Cu(In,Ga)Se2 solar cells under front and rear illuminations, *Solar Energy*, 218, 76-84,2021

[55] Wenjie Li, Ye Feng, Chunlei Yang, Numerical analysis of the back interface for high efficiency wide band gap chalcopyrite solar cells, *Solar Energy*, 180, 207-215, 2019

[56] P.K. Kalita, B. Barman,Influence of back surface field layer on enhancing the efficiency of CIGS solar cell, *Solar Energ*, 216, 329-337, 2021

[57] M. Mostefaouia,b, H. Mazaria, S.Khelifia, b , A.Bouraioua, R.Daboua, Simulation of High Efficiency CIGS solar cells with SCAPS-1D software , *Energy Procedia*,74, August 2015, 736-744

[58] M. Moradi, R. Teimouri, M. Saadat, M. Zahedifar, Buffer layer replacement: A method for increasing the conversion efficiency of CIGS thin film solar cells, *Optik*, 136, 2017, 222-227, ISSN 0030-4026,

[59] H. Helmers, C. Karcher, A.W. Bett, Bandgap determination based on electrical quantum efficiency, *Appl. Phys. Lett.*, 103, (2013) 032108.

[60] M. Troviano, K. Taretto, Temperature-dependent quantum efficiency analysis of graded-gap Cu(In,Ga)Se2 solar cells, *Sol. Energy Mater. Sol. Cells*, 95, (2011) 3081–3086.

[61] W. Hörig, H. Neumann, H. Sobotta, B. Schumann, G. Kühn, The optical properties of CuInSe2 thin films, *Thin Solid Films*, 48, 67–72, (1978).

[62] E.Klampaftis,D.Ross,K.R.McIntosh,B.S.Richards,Enhancing the performance of solar cells via luminescent down-shifting of the incident spectrum:a review,Sol.*Energy Mater.Sol.Cells*, 93, 1182–1194,(2009).

[63] B.S.Richards,Enhancing the performance of silicon solar cells via the application of passive luminescence conversion layers,*Sol.Energy Mater.Sol.Cells*, 90,2329–2337,(2006).

[64] Nima Khoshsirat,Copper-Indium-Gallium-diSelenide (CIGS) Nanocrystalline Bulk Semiconductor as the Absorber Layer and Its Current Technological Trend and Optimization, *IntechOpen*, , 2016.

[65] Q. Cao, O. Gunawan, M. Copel, K. B. Reuter, S. J. Chey, V. R. Deline, et al., "Defects in Cu (In, Ga) Se2 chalcopyrite semiconductors: a comparative study of material properties, defect states, and photovoltaic performance,*Advanced Energy Materials*, 1, 845–853, 2011.

[66] J. Pohl, T. Unold, and K. Albe, "Antisite traps and metastable defects in Cu (In, Ga) Se2 thin-film solar cells studied by screened-exchange hybrid density functional theory," arXiv preprint arXiv:1205.2556, 2012.

[67] B. Huang, S. Chen, H.-X. Deng, L.-W. Wang, M. A. Contreras, R. Noufi, et al., "Origin of reduced efficiency in Cu (In, Ga) Se solar cells with high Ga concentration: alloy solubility versus intrinsic defects," , *IEEE Journal of Photovoltaic*, 4, 477–482, 2014.

[68] Heo, S. et al. Defect visualization of Cu(InGa)(SeS)2 thin films using DLTS measurement. *Scientific Reports*, 6, 30554;

[69] Oana Cojocaru-Miredin et al. Characterization of Grain Boundaries in Cu(In,Ga)Se2 Films Using Atom-Probe Tomography, *IEEE Journal of photovoltaics*, 1 (2), 207-212, (2011).

[70] L. E. Oikkonen, M. G. Ganchenkova, A. P. Seitsonen R. M. Nieminen. Effect of sodium incorporation into CuInSe2 from first principles, *J. Appl. Phys.*, 114, 083503 (2013).

[71] Gregory Brown, Vladimir Faifer, Alex Pudov, Sergey Anikeev, Eugene Bykov, Miguel Contreras, and Junqiao Wu, Determination of the minority carrier diffusion length in compositionally graded Cu,,In,Ga...Se2 solar cells using electron beam induced current, *Appl. Phys. Lett.*, 96, 022104 (2010);

[72] Devi, C. Mehra, R. Device simulation of lead-free MASnI3 solar cellwith CuSbS2 (copper antimony sulfide). *J. Mater. Sci.*. 54, 5615–5624 (2019).

 doi:10.20944/preprints202110.0326.v2

[73] APL Mater. 6, 096103 (2018); https://doi.org/10.1063/1.5042046